Biological Journal of the Linnean Society, 2020, **130**, 178–194. With 4 figures.

Cranial integration in the fire salamander, *Salamandra salamandra* (Caudata: Salamandridae)

MARGOT BON[1,*,†], CARLA BARDUA[1,2,*,†], ANJALI GOSWAMI[1], and ANNE-CLAIRE FABRE[1,*]

[1]*Department of Life Sciences, Natural History Museum, Cromwell Rd, Kensington, London, SW7 5BD, UK*
[2]*Department of Genetics, Evolution & Environment, University College London, Gower St, Bloomsbury, London, WC1E 6BT, UK*

Received 5 November 2019; revised 4 February 2020; accepted for publication 6 February 2020

Phenotypic integration and modularity are concepts that represent the pattern of connectivity of morphological structures within an organism. Integration describes the coordinated variation of traits, and analyses of these relationships among traits often reveals the presence of modules, sets of traits that are highly integrated but relatively independent of other traits. Phenotypic integration and modularity have been studied at both the evolutionary and static level across a variety of clades, although most studies thus far are focused on amniotes, and especially mammals. Using a high-dimensional geometric morphometric approach, we investigated the pattern of cranial integration and modularity of the Italian fire salamander (*Salamandra salamandra giglioli*). We recovered a highly modular pattern, but this pattern did not support either entirely developmental or functional hypotheses of cranial organisation, possibly reflecting complex interactions amongst multiple influencing factors. We found that size had no significant effect on cranial shape, and that morphological variance of individual modules had no significant relationship with degree of within-module integration. The pattern of cranial integration in the fire salamander is similar to that previously recovered for caecilians, with highly integrated jaw suspensorium and occipital regions, suggesting possible conservation of patterns across lissamphibians.

ADDITIONAL KEYWORDS: Amphibia – crania – disparity – morphology – phenotypic integration.

INTRODUCTION

Identifying the primary factors that shape the evolution of organisms is a long-standing interest in biology. Analysing phenotype is a relevant scale to address this question, allowing consideration of both external (e.g. ecological interactions, climate) and internal (i.e. genetic, developmental) factors (e.g. Collar *et al.*, 2010; Moen *et al.*, 2013; Goswami *et al.*, 2014; Da Silva *et al.*, 2018). However, the types and sources of the data used by studies of external or internal factors are usually different, preventing combined studies of both aspects (Goswami *et al.*, 2014). In 1958, Olson and Miller hypothesised that phenotypic traits are more integrated or correlated (statistically associated) when derived from the same genetic or developmental origin or participating in the same function (Oslon & Miller, 1958). Organisms are made of locally integrated units, also defined by Wagner (1996) as modules, which has also been noted as the reason why characters are often easily identifiable across diverse organisms (Wagner & Altenberg, 1996). Traits within a module are highly connected (i.e. integrated) but less connected to traits of other modules. Integration and modularity therefore refer to the pattern and magnitude of connectivity within an organism. It has been suggested that modularity enables sets of traits to evolve independently of other sets of traits, reducing or removing the constraints of high integration, where changes in one trait may negatively impact the function of a closely integrated trait (Wagner, 1996). Empirical studies have focused on this aspect of evolutionary integration and modularity and have showed either positive correlations between the magnitude of integration and rate of evolution or disparity (Goswami *et al.*, 2014; Randau & Goswami, 2017), or that high integration is indeed correlated

*Corresponding authors. E-mail: m.bon@nhm.ac.uk; ucbtcb5@ucl.ac.uk; a.fabre@nhm.ac.uk
†These authors contributed equally to this work

with low evolutionary rates (Felice *et al.*, 2018). More recent studies have also found no simple linear relationship between strength of integration and either evolutionary rate or disparity (Bardua *et al.*, 2019b, Watanabe *et al.*, 2019).

Integration and modularity can be explored at the evolutionary level (i.e. at the interspecific level across a whole clade at one ontogenetic stage (Klingenberg, 2014)), the static level (i.e. at the intraspecific level, within one species at one ontogenetic stage (Klingenberg, 2014)) and the ontogenetic level (i.e. within one species across ontogenetic stages (Klingenberg, 2014)). Study of these three levels reveals insights into the underlying biological processes governing evolution. The static level can be used to infer functional, developmental and genetic integration (Klingenberg, 2014), all of which mutually influence each other, forming a complex network of interactions (see Klingenberg (2008: fig. 1)). Functional and genetic modularity are thought to evolve to match, through the creation of a modular 'genotype-phenotype map' (Wagner & Altenberg, 1996), and it is hypothesised that developmental pathways evolve so that functional and developmental integration also match ('matching hypothesis' (Wagner & Altenberg, 1996)). Thus, identification of the pattern of static integration can serve as a starting point to then determine functional, genetic and developmental sources of covariation within a structure and how these factors influence evolvability (Klingenberg, 2014). Evolutionary integration reveals the large-scale patterns of change during evolution, which can be driven by both functional (e.g. performance selection) and genetic (e.g. evolution by selection and drift) modularity (Klingenberg, 2008). Concordant patterns within and between species suggest that modularity is affected by common biological processes through evolution (e.g. developmental, genetic), as has been found in compound leaves where development highly modulates any other variation (Klingenberg *et al.*, 2012). Conversely, discrepancy in patterns of integration between evolutionary and static levels has been found in lizards, suggesting that the functional integration pattern at the static level has appeared by adaptation through selection (Urošević *et al.*, 2019). Finally, selection can act on any ontogenetic stage and studies have demonstrated that patterns of integration shift through ontogeny (Zelditch, 1988; Zelditch & Carmichael 1989a,b; Ackermann, 2005; Willmore *et al.*, 2006; Goswami & Polly, 2010a; Goswami *et al.*, 2012). All three levels of integration and modularity can therefore together aid our understanding of evolution.

Within tetrapods (limbed vertebrates), evolutionary, ontogenetic and static modularity have been investigated across a range of taxa. Evolutionary modularity has been investigated in mammals, where many studies found as many as six modules in the cranium (e.g. Cheverud, 1995; Goswami, 2006; Porto *et al.*, 2009; Goswami & Polly, 2010b), influenced by both development and function. Six-module cranial organisation was also recovered at the static and the ontogenetic levels, for example in macaques (Goswami & Finarelli, 2016), suggesting that modularity in the mammal cranium is constrained by both functional and developmental influences. Within archosaurs, patterns of evolutionary modularity are generally conserved, with highly modular systems recovered across the crania of birds, non-avian dinosaurs and crocodylomorphs (Felice & Goswami, 2018; Felice *et al.*, 2019). Alternatively, the avian skull has also been found to be highly integrated at the evolutionary level (Klingenberg & Marugán-Lobón, 2013). Across squamates, Watanabe *et al.* (2019) found that the cranium comprised nine modules in snakes and ten modules in lizards, revealing highly modular structures influenced by functional constraints across these clades. In contrast, at the static level, Urošević *et al.* (2012) found that the head of the common lizard (*Podarcis muralis*) is a highly integrated structure. Patterns of cranial integration across lacertids (lizards) have been found to vary across evolutionary and static levels, with patterns at the evolutionary level more influenced by development and patterns at the static level more influenced by function, which suggests that functional modularity is adaptive (Urošević *et al.*, 2019). In *Anolis* lizards, patterns of static modularity have also been found to vary across species; a three-module cranial organisation is supported in *Anolis* species but no support for modular organisation was found in other *Anolis* species. Thus, similar to lacertids (Urošević *et al.*, 2019), patterns of cranial integration in *Anolis* lizard species may be evolutionary flexible and influenced by unique functional pressures acting on the diverse cranial shapes (Sanger *et al.*, 2012). Across amniotes, studies of evolutionary and static modularity have therefore recovered a range of modular organisations, from fully integrated to highly modular structures, although differences in results may partially reflect differences in the type of data collected (Felice *et al.*, 2018; Goswami *et al.*, 2019).

Relatively few studies have focused on lissamphibians (Anura, Caudata and Gymnophiona). The large range of ecologies and developmental histories across lissamphibians, along with their impressive cranial diversity, suggest patterns of cranial integration in this clade may be complex. However, studies of European newts at the static level have found that the skull is highly integrated with no distinct modules (Ivanović *et al.*, 2005; Ivanović & Kalezić, 2010), a result mirrored at the evolutionary level across the myobatrachid frog family (Vidal-García & Keogh, 2017). Interestingly, static integration of the cranium is lower for paedomorphic forms of two European newts compared with fully metamorphosed forms, which

can be explained by ontogenetic integration, where integration increases post-metamorphosis (Ivanović *et al.*, 2005). Mixed support was found for a range of three- to five module models across different toad species of the *Rhinella granulosa* complex (Simon & Marroig, 2017), and for caecilians, a two-module model was found as best supported for the skull at both the evolutionary and static level (Sherratt, 2011). However, comparison of patterns of integration across clades is hindered by the range of data types, from linear distances (e.g. Simon & Marroig, 2017) to landmarks (e.g. Sherratt, 2011), and some methods prohibit the exploration of multiple models of modularity. Recent advancements in morphometric methods may facilitate the detection of a finer-scale modular signal. Recent high-dimensional studies across caecilians (Bardua *et al.*, 2019b) and within two caecilian species (Marshall *et al.*, 2019) have both recovered similarly highly modular cranial structures, suggesting possible conservation of modularity across static and evolutionary levels. Thus investigation into finer-scale patterns of static and evolutionary integration for additional lissamphibian groups may reveal whether this pattern is conserved across Lissamphibia.

Caudata (salamanders) comprises ten ecologically and morphologically diverse families and displays a tremendous range of life cycle strategies (e.g. Bonett *et al.*, 2013; Bonett & Blair, 2017; Bonett, 2018; Ledbetter & Bonett, 2019). Extensive phenotypic variation can also extend intraspecifically in salamanders, as in the fire salamander *Salamandra salamandra* (Linnaeus, 1758) which exhibits a range of morphologies, colour patterns and reproductive strategies depending on the subspecies (Sparreboom, 2014; Beukema *et al.*, 2016). Taxonomy of the fire salamander is repeatedly being revised, but *S. salamandra* currently comprises at least ten subspecies (Sparreboom, 2014). Across these subspecies, the fire salamander is polymorphic in its mode of reproduction, with most populations ovoviviparous but some viviparous (Dopazo & Alberch, 1994; Alcobendas *et al.*, 1996; Buckley *et al.*, 2007). The high flexibility in development in this species suggests developmental influences on cranial integration may be variable, and provides an interesting opportunity for investigating developmental and functional hypotheses of static modularity. The skull is suitable for investigating patterns of integration, as it is a highly developmentally complex structure (Hanken & Hall, 1993), given the different embryonic origins (neural crest and paraxial mesoderm) and types of ossification (endochondral and intramembranous) across the cranial regions. In addition, the transition from larval to adult morphology for metamorphic subspecies involves deep osteological remodelling in the skull, including the resorption of bones (e.g. vomer and palatine portion of the palatopterygoid), and the late development of the maxilla and prefrontal (Rose, 2003). The cranium of *S. salamandra* comprises 15 bones, although three of them fuse into one single complex - the prootic and opisthotic fuse to form the otic capsule, which fuses posteriorly with the exoccipital and forms the occipito-otic bone (Rose, 2003). Apart from three endochondral bones (the occipito-otic complex, the orbitosphenoid and the quadrate), all bones form by intramembranous ossification (Rose, 2003). The skull is also functionally complex (Moore, 1981; Hanken & Hall, 1993), playing a major role in foraging and feeding, as well as protecting the brain and housing the organs that perceive the main senses (hearing, sight, smell and taste). The skull is therefore an ideal system for investigating fine-scale patterns of integration.

Here we investigate patterns of morphological integration and modularity in the skull of the Italian subspecies of fire salamander [*Salamandra salamandra giglioli* (Eiselt & Lanza, 1956)], which undergoes metamorphosis (Seidel & Gerhardt, 2016). We directly compare eight different modular structures based on hypothesised functional and developmental relationships between cranial regions. We also determine whether integration constrains or facilitates morphological diversity (disparity) by quantifying the relationship between within-module variance and within-module magnitude of integration. Combined, these analyses allow us to assess static (intraspecific) modularity and integration within a population, for qualitative comparison to previous studies of modularity and integration within lissamphibians [e.g. in caecilians (Bardua *et al.*, 2019b; Marshall *et al.*, 2019), frogs and toads (Simon & Marroig, 2017; Vidal-García & Keogh, 2017) and salamanders and newts (Ivanović *et al.*, 2005; Ivanović & Kalezić, 2010)] and amniotes. This study thus adds to a rich and increasing pool of understanding the evolution and significance of phenotypic integration and modularity for shaping organismal variation at micro- and macroevolutionary scales.

MATERIAL AND METHODS

Study specimens

The sample analysed in this study includes 40 specimens of the subspecies *S. salamandra gigliolii* (Supporting Information, Table S1). None of the cloacal regions of the specimens displayed an obvious swelling that could differentiate males from females (Brizzi & Calloni, 1992), thus sex information was not available for these specimens. All the specimens were preserved in alcohol in the collections of the Natural History Museum (NHM), London. The specimens were imaged using micro CT-scanning (Nikon Metrology X-Tek HMX ST 225) at the NHM and resulting tomographs were further segmented in Avizo Lite v.9.3 (FEI, Hillsboro, OR, USA) to obtain 3D models of the crania.

Because this study focuses on cranial morphology, the reconstructed meshes were processed in Geomagic Wrap (3D Systems [Copyright © 2020 3D Systems, Inc.]) to remove vertebral elements and the mandible from each cranium, which could hinder access to the surface of interest. The right half of each skull was then prepared for surface analyses using Geomagic Wrap, by smoothing noise introduced from scanning and removing holes that could prevent the acquisition of surface details (Bardua *et al.*, 2019a). The quality of the left side of the skull was favoured in two specimens, for which the skull was thus mirrored with the "Mirror" function in Geomagic Wrap.

Morphometric data

To characterise the shape of the regions of interest and assess how they correlate, a landmarking procedure was performed using Checkpoint (Stratovan, Davis, CA, USA) by the same user to keep the placement of landmarks consistent and to avoid user bias. Eighty-five anatomical landmarks were manually placed on the right side of each skull, defining 20 regions in total (Fig. 1 and Table 1) that were identifiable in all specimens of the dataset. These landmarks were homologous across all specimens. Regions delineate bones, or sub-regions of bones when the bone is anatomically polyvalent (e.g. with ventral and dorsal surfaces), and thus potentially modular due to differing functional pressures. The regions are delimited with sliding semilandmarks ('curves') in between landmarks (Fig. 1 and Supporting Information (Table S2)). Eighty-five curves in total were drawn over the skull. These curves were then resampled in R (R Core Development Team, 2019) to 689 curve semilandmarks to ensure that they were equidistant and that they capture shape optimally (Botton-Divet *et al.*, 2016). To capture surface information from the regions, 375 sliding surface points were placed over the crania following a semi-automatic procedure using the R (R Core Development Team, 2019) package *Morpho* v.2.6 (Schlager, 2017). First, one specimen of the dataset was defined as the template and surface points were manually placed onto each region. Then, surface points were semi-automatically projected from this template onto each specimen with the "placePatch" function in *Morpho* v.2.6 (Schlager, 2017). Finally, all curve and surface points were slid to become geometrically homologous, minimizing the bending energy criterion, using the "slider3d" function in *Morpho* v.2.6 (Schlager, 2017). A detailed description of this method is available in Bardua *et al.* (2019a).

Following sliding, morphometric data were subjected to Procrustes analysis to remove the non-shape aspects of isometric size, rotation and translation (Rohlf & Slice, 1990). However, because alignment of only one side of a bilateral structure can have a negative impact on the Procrustes alignment (Cardini, 2016), we first mirrored morphometric data to produce a fully bilateral configuration using the "mirrorfill" function in *paleomorph* v.0.1.4 (Lucas & Goswami, 2017). We then performed Procrustes alignment with the "gpagen" function in *geomorph* v.3.0.4 (Adams *et al.*, 2019). Finally, the mirrored side was removed from the resulting Procrustes shape coordinates, leaving the right side coordinates only for further analyses.

Allometry

Allometry corresponds to the impact of size on shape (Klingenberg, 2016). In our study, cranial size was measured as the centroid size (Klingenberg, 2016),

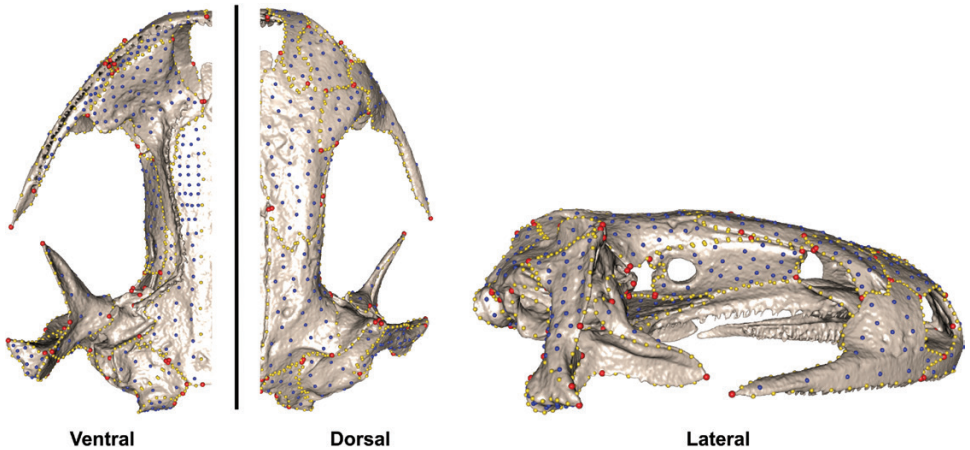

Figure 1. Landmark and semilandmark positions on the cranium, in ventral, dorsal and lateral views, shown on a fire salamander *S. salamandra gigliolii* (NHM 1911.2.22.62). Points are colour-coded as follows: landmarks (red), curve semilandmarks (yellow) and surface semilandmarks (blue).

Table 1. Anatomical landmark definition

	Landmark position
1	Premaxilla, *pars frontalis*: anteroventral extreme
2	Premaxilla, *pars frontalis*: ventrolateral extreme
3	Premaxilla, *pars frontalis*: posterior extreme of the suture with the nasal
4	Premaxilla, *pars frontalis*: posterior extreme of the intersection between the ventral and medial borders of the external naris
5	Maxilla, *pars fascialis*: anteroventral extreme
6	Maxilla, *pars fascialis*: posteroventral extreme
7	Maxilla, *pars fascialis*: anterodorsal extreme
8	Maxilla, *pars fascialis*: dorsal extreme
9	Parasphenoid, anterior extreme, midline
10	Parasphenoid, posterior extreme of the suture with the orbitosphenoid
11	Parasphenoid, anterior extreme of the suture with the otic bone
12	Parasphenoid, point at the maximum of concavity between 11 and 13
13	Parasphenoid, posterior extreme, midline
14	Squamosal, posterodorsal extreme, in contact with the otic capsule
15	Squamosal, posteroventral extreme
16	Squamosal, anterodorsal extreme, in contact with the otic capsule
17	Squamosal, point at the maximum of convexity of the anterior border of the squamosal
18	Squamosal, anteroventral extreme
19	Squamosal, posteroventral extreme of the suture with the otic bone
20	Pterygoid, posterodorsal extreme, laying close to the quadrate
21	Pterygoid, point at the maximum of concavity between 20 and 22
22	Pterygoid, most medial point of the pterygoid
23	Pterygoid, anterior extreme of the ascending process
24	Pterygoid, point at the maximum of concavity between 23 and 25
25	Pterygoid, posteroventral extreme, situated close to the quadrate
26	Frontal, anteromedial extreme of the suture with the *pars frontalis* of the premaxilla
27	Frontal, anterolateral extreme
28	Parietal, point at the intersection with the most anterodorsal part of the prootic
29	Parietal, posterolateral extreme
30	Parietal, posteromedial extreme
31	Premaxilla, *pars palatina*: anteromedial extreme
32	Premaxilla, *pars palatina*: anterolateral extreme
33	Premaxilla, *pars palatina*: posterolateral extreme
34	Premaxilla, *pars palatina*: posteromedial extreme
35	Maxilla, *pars palatina*: anteromedial extreme
36	Maxilla, *pars palatina*: posteromedial extreme
37	Maxilla, *pars palatina*: posterolateral extreme
38	Nasal, anterior extreme of the suture with the *pars frontalis* of the premaxilla
39	Nasal, posterior extreme of the suture with the prefrontal
40	Nasal, anterior extreme of the suture with the maxilla
41	Occipital, anteromedial extreme
42	Occipital, dorsal extreme of the foramen magnum
43	Occipital condyle, dorsal extreme of the junction with the foramen magnum
44	Occipital condyle, ventral extreme of the junction with the foramen magnum
45	Occipital, medial extreme of the articular facet
46	Occipital, posteroventral extreme of the suture with the parasphenoid
47	Otic capsule, dorsal extreme of the foramina for cranial nerve X
48	Otic capsule, posteroventral extreme of the suture with the parasphenoid
49	Most anteroventral point of the prootic
50	Otic capsule, ventral extreme of the foramina for cranial nerve X
51	Vomer, anteromedial extreme of the ventral side

Table 1. Continued

	Landmark position
52	Vomer, anterolateral extreme of the ventral side
53	Vomer, posterior extreme of the ventral side
54	Vomer, anteromedial extreme of the ventral side
55	Occipital, lateral extreme of the articular facet
56	Occipital, anteroventral extreme of the suture with the parasphenoid, in contact with 48 and 12
57	Occipital, ventral extreme of the foramina for cranial nerve X
58	Occipital, dorsal extreme of the foramina for cranial nerve X
59	Occipital, point at the intersection with the parietal and the opisthotic
60	Otic capsule, ventral extreme of the inner suture of the fenestra ovalis, at the intersection between the opisthotic and prootic
61	Otic capsule, point at the intersection with the parietal and the occipital
62	Otic capsule, anterodorsal extreme of the prootic
63	Squamosal, antero-ventro-medial extreme
64	Otic capsule, dorsal extreme of the inner suture of the fenestra ovalis, at the fusion between the opisthotic and prootic
65	Occipital, posteromedial extreme
66	Jaw joint, posterior extreme of the articulation
67	Jaw joint, anterior extreme of the articulation
68	Jaw joint, anteromedial extreme of the articulation
69	Quadrate, anterodorsal extreme, at the intersection with the squamosal
70	Otic capsule, most dorsal point of the ventral side of the anterior ridge of the prootic
71	Quadrate, anterior extreme of the medio dorsal margin
72	Parietal, anterolateral extreme
73	Parietal, anteromedial extreme
74	Frontal, posterolateral extreme
75	Frontal, posteromedial extreme
76	Otic capsule, most ventral point of the dorsal side of the anterior ridge of the prootic
77	Quadrate, posterodorsal extreme, at the intersection with the squamosal
78	Orbitosphenoid, posterodorsal extreme
79	Orbitosphenoid, anterodorsal extreme
80	Orbitosphenoid, anteroventral extreme
81	Orbitosphenoid, posteroventral extreme
82	Prefrontal, anterolateral extreme
83	Prefrontal, anteromedial extreme
84	Prefrontal, posterior extreme
85	Prefrontal, posterolateral extreme

which was calculated with the "gpagen" function in *geomorph* v.3.0.4 (Adams *et al.*, 2019) during the Procrustes alignment (see Supporting Information, Table S3). Allometry was assessed with a regression of the shape data on log-transformed centroid size, using the "procD.allometry" function in *geomorph* v.3.0.4 (Adams *et al.*, 2019).

Modularity and integration

The eight hypothetical patterns of modularity tested in this study are outlined below. Most simply, we tested for a fully integrated cranium (Fig. 2A and Table 2). The cranium could also be divided into two modules based on the two types of ossification (endochondral and dermal), resulting in two different developmental modules (Fig. 2B and Table 2). We also tested two functional hypotheses that were previously tested for caecilians (Bardua *et al.*, 2019b; Marshall *et al.*, 2019), in which the skull is either dorsoventrally divided (Fig. 2C and Table 2) or partitioned into four functional modules (Fig. 2D and Table 2). Since bones have different ossification sequences, which could influence skull variation and evolution, we hypothesised that cranial modules are defined by their time of ossification (Fig. 2E and Table 2) as previously explored in the literature (Ivanović & Kalezić, 2010), resulting in four different modules: early, mid and late ossification and bones remodeled during metamorphosis. We further partitioned and tested a seven-module model (Fig. 2F

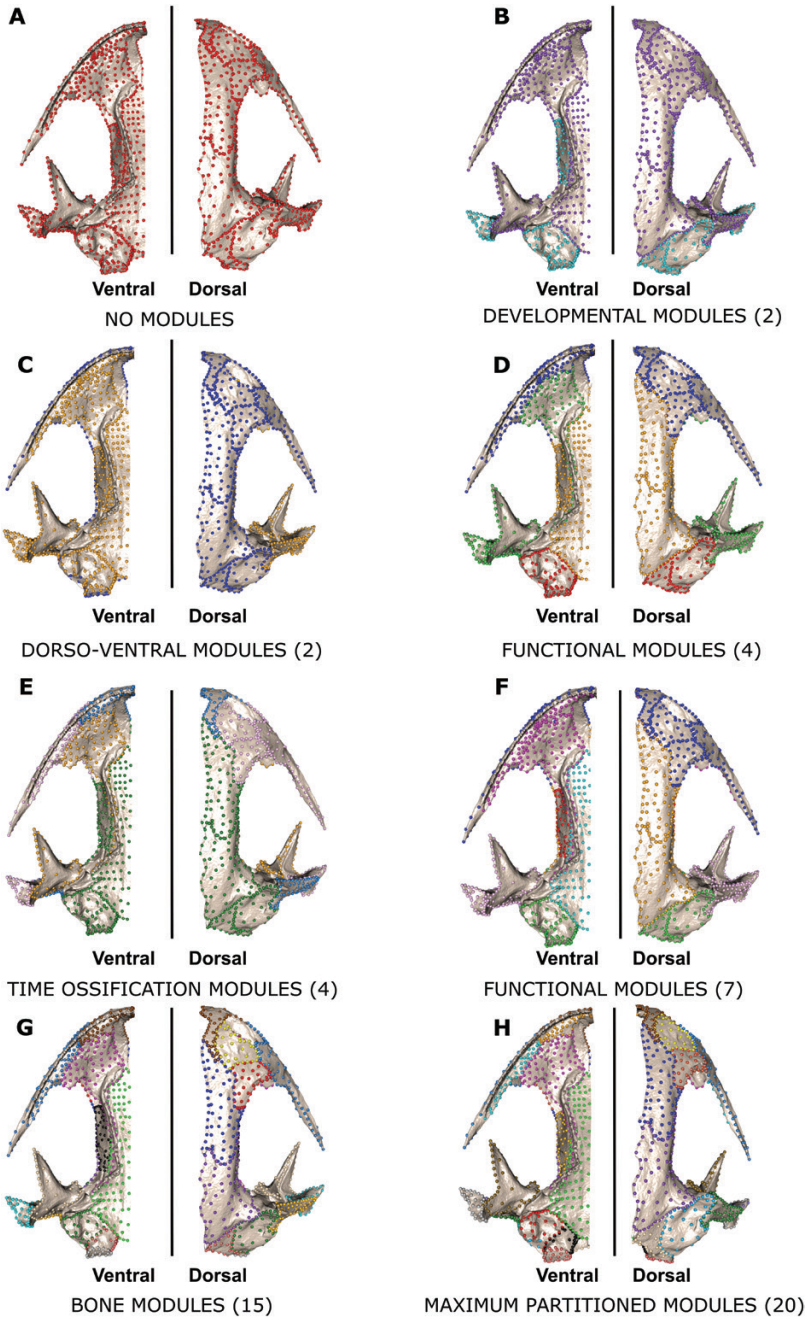

Figure 2. Hypotheses of modular patterns tested in EMMLi analysis. All of the landmarks and semilandmarks from each region were assigned to hypothesised modules and colour-coded accordingly. A, no module model (no modular organisation); B, developmental module model (dermal: purple, endochondral: blue); C, dorso-ventral module model (dorsal: blue, ventral: yellow); D, 4 functional module model (snout: blue, braincase: yellow, jaw suspension: green, occipital-otic complex: red); E, time of ossification module model (early development: blue, mid-development: green, late development: light pink, metamorphosis: yellow); F, 7 functional module model (snout: navy blue, floor of the braincase: light blue, jaw suspension: light pink, skull roof: yellow, palatine: magenta, occipital-otic complex: green, lateral side of the braincase: red); G, bone module model (frontal: dark blue, maxilla: blue, nasal: yellow; occipital: peach, occipital condyle: grey, orbitosphenoid: black, otic: green khaki, parasphenoid: green, parietal: violet, prefrontal: red, premaxilla: brown, pterygoid: egg shell, quadrate: cyan, squamosal: gold, vomer: hot pink); H, maximum partitioned module model (frontal: dark blue, jaw joint: grey, maxilla: blue, maxilla ventral: cyan, nasal: yellow; occipital dorsal: egg shell, occipital ventral: black, occipital condyle: peach, orbitosphenoid: light orange, otic dorsal: light blue, otic ventral: black, parasphenoid: green, parietal: dark violet,

and Table 2) similar to the model found in mammals (Goswami, 2006). Each bone is an identifiable unit that originates from an independent signal, so we also hypothesised that bones comprise their own modules (Fig. 2G and Table 2). Finally, because some bones form distinct regions that are implied in different functions (e.g. the *pars facialis* and the *pars palatina* of the maxilla) and are thus potentially functionally modular, we further hypothesised that the cranium could be highly partitioned into 20 modules (Fig. 2H and Table 2).

Modularity was investigated with two different approaches. Firstly, we conducted EMMLi ('Evaluating Modularity with Maximum Likelihood') analysis. For this, congruence coefficients were calculated with the "EMMLi" function from the *EMMLi* v.0.0.3 R package (Goswami *et al.*, 2017). Robustness of the results was tested with a random subsampling down to 10% of the full data, and EMMLi ran iteratively 100 times, using the "subSampleEMMLi" function from the *EMMLi* v.0.0.3 R package. Mean results from the 100 subsamples were then compared to the analysis of the full dataset.

Secondly, we conducted Covariance Ratio (CR) analysis (Adams, 2016) using the "modularity.test" function from the *geomorph* v.3.0.4 R package. Although EMMLi is a model selection approach that compares different models of modular organisation and outputs the most likely model along with its between- and within-module correlations, covariance ratio analysis is a hypothesis testing method that calculates the covariance ratio between the different regions in one specific model. The ratio is the total between-module covariance over the within-module covariance (Adams, 2016), meaning that a ratio of one reflects a lack of modularity. Therefore, support for the preferred model from EMMLi analysis was assessed by calculating the covariance ratio of that model, to confirm that both methods supported similar patterns of trait integration and modularity. We further conducted both analyses with a landmark-only dataset for comparison.

Morphological variance

To discern how each module varies across the crania, we computed the shape variance (the Procrustes distance between shapes and the mean shape) of each module with the "morphol.disparity" function from the *geomorph* v.3.0.4 R package. To compare the variances between modules, each variance was corrected by dividing by the total number of landmarks defined in the module concerned.

To investigate the relationship between shape variance and the magnitude of within-module integration, we computed a linear regression of corrected variances on within-module correlation.

RESULTS

Allometry

The regression of shape on log-transformed centroid size was not significant ($R^2 = 0.037$, $P = 0.125$), suggesting that there is no significant effect of size on shape in the fire salamander cranium. Therefore, we did not apply allometric corrections in further analyses.

Modularity and integration

The most supported model from EMMLi for the complete dataset was the maximal partitioning modular pattern (Table 3), comprising 20 modules (Fig. 3). However, since we could not test all possible models of modularity, and because previous analyses have suggested that EMMLi has a tendency to pick the most-parametrised model with semilandmark data, we explored the correlation (rho) values among and within modules to assess possible further groupings of modules into larger modules, following the method previously described (Felice & Goswami, 2018; Bardua *et al.*, 2019b; Marshall *et al.*, 2019). Modules were hence further grouped when the between-module estimated correlation was within 0.1 of the smallest within-module trait correlation of the module pair under question. Therefore, we grouped 11 regions into four larger modules, as follows: the squamosal, the pterygoid, the jaw joint and the quadrate were grouped into one jaw suspensorium module, the ventral and dorsal regions of the premaxilla formed a second module, the ventral and dorsal regions of the maxilla a third module, and the ventral and dorsal part of the occipital were grouped with the occipital condyle (Fig. 3 and Table 3). The average random 10% subsampling of the data resulted in a near-identical pattern of trait integration (Supporting Information, Table S4) compared with the full data, confirming the robustness of our results. Through this approach we recovered a 13-module model as best supported.

EMMLi analysis of the landmark-only dataset supported the 15-module model (which subdivided the

prefrontal: orange, premaxilla dorsal: dark gold, pterygoid: golden brown, quadrate: light violet, squamosal: green khaki, vomer: magenta). For further details about the results on modularity, please see Tables 3, 4 and Supporting Information (Tables S3-S5).

Table 2. Hypotheses of modular patterns tested in EMMLi analysis: No module (no modular organisation); developmental modules (1: dermal, 2: endochondral); dorsoventral modules (1: dorsal, 2: ventral); four functional modules (1: snout, 2: braincase, 3: jaw suspension, 4: occipital-otic complex); time ossification modules (1: early development, 2: mid-development, 3: late development, 4: metamorphosis); seven functional modules (1: snout, 2: floor of the braincase, 3: jaw suspension, 4: skull roof, 5: palatine, 6: occipital-otic complex, 7: lateral side of the braincase); bone modules (each bone is a module); maximum partitioned modules (each region is a module)

Region	No modules	Developmental modules	Dorsoventral modules	Four functional modules	Time ossification modules	Seven functional modules	Bone modules	Maximum partitioned modules
Occipital condyle	1	2	1	4	2	6	10	12
Frontal	1	1	1	2	2	4	6	3
Maxilla, dorsal	1	1	1	1	3	1	2	5
Maxilla, ventral	1	1	2	1	3	5	2	9
Nasal	1	1	1	1	3	1	8	10
Occipital, dorsal	1	2	1	4	2	6	9	11
Occipital, ventral	1	2	2	4	2	6	9	13
Orbitosphenoid	1	2	2	2	2	7	14	17
Otic region, dorsal	1	2	1	4	2	6	11	20
Otic region, ventral	1	2	2	4	2	6	11	14
Parietal	1	1	1	2	2	4	7	4
Premaxilla, dorsal	1	1	1	1	1	1	1	1
Premaxilla, ventral	1	1	2	1	1	5	1	2
Prefrontal	1	1	1	2	3	1	15	18
Parasphenoid	1	1	2	2	2	2	3	6
Pterygoid	1	1	2	3	4	3	5	8
Quadrate	1	2	2	3	3	3	13	16
Jaw joint	1	2	2	3	3	3	13	19
Squamosal	1	1	2	3	1	3	4	7
Vomer	1	1	2	3	4	5	12	15

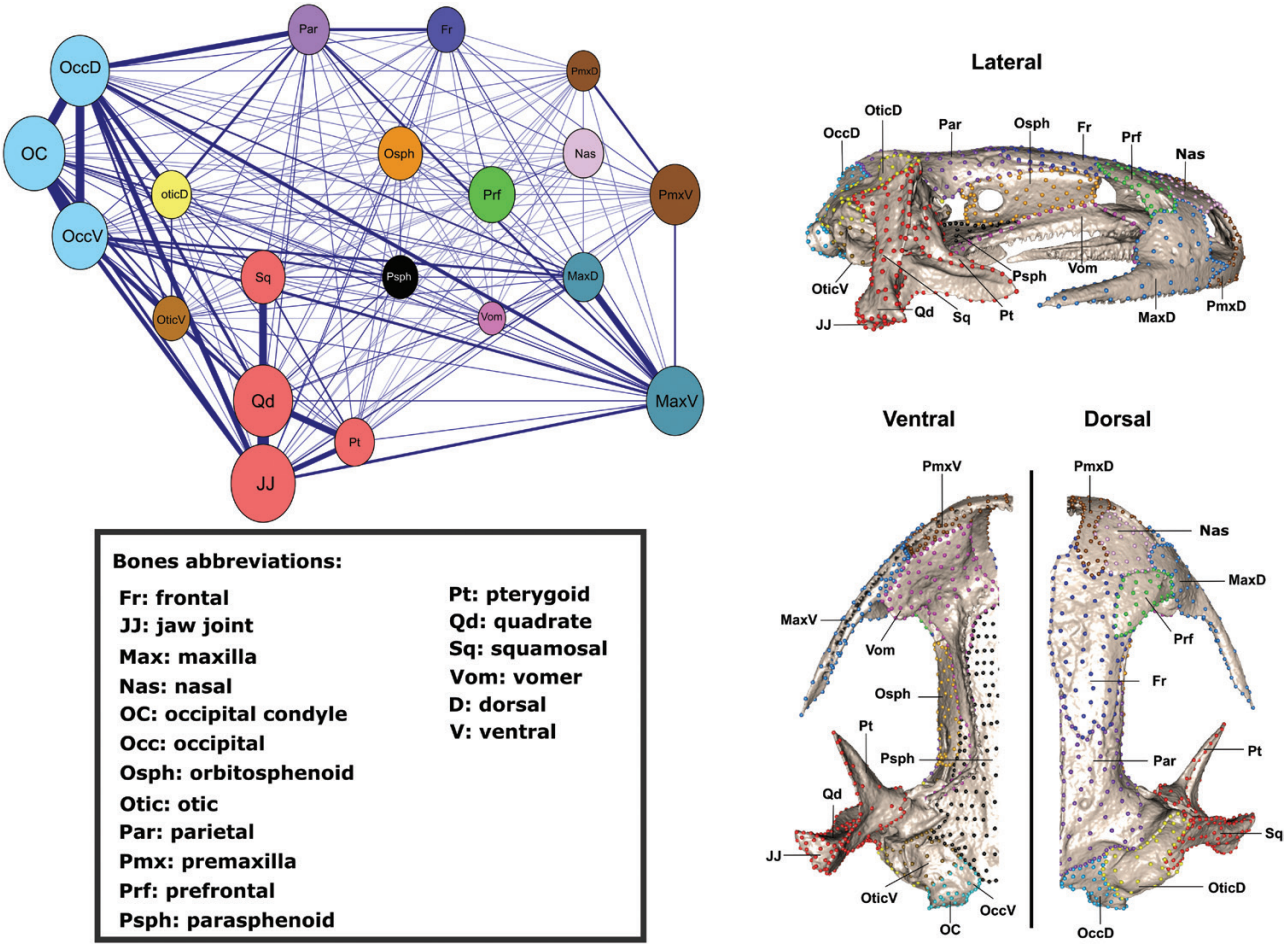

Figure 3. The thirteen-module model identified with EMMLi analysis. Top left, network graph of the 20 cranial regions defined in this study, coloured in the thirteen modules identified from EMMLi analysis. The network displays a right-hand side lateral view of the skull. The thickness of a line and the size of a circle respectively correspond to the strength of integration between and within modules. At the right side of the figure, the resulting thirteen modules are visualised on a specimen (*S. salamandra gigliolii* NHM 1911.2.22.62) in lateral, ventral and dorsal views. The thirteen modules correspond to the following regions: occipital in light blue, dorsal (OccD) and ventral (OccV) part of the occipital bone and condyle (OC); dorsal otic (OticD) in yellow and ventral otic (OticV) in light brown; jaw suspension module with squamosal (Sq), quadrate (Qd), jaw joint (JJ) and pterygoid (Pt) in red; parasphenoid (Psph) in black; vomer (Vom) in magenta; orbitosphenoid (Osph) in orange; prefrontal (Prf) in green; Maxilla in blue with the dorsal (MaxD) and ventral (MaxV) sides; premaxilla in brown with dorsal (PmxD) and ventral (PmxV) sides; nasal (Nas) in pale pink; frontal (Fr) in dark blue; parietal (Par) in dark purple.

cranium according to osteological units). However, further assessment of the within- and between-module rho values revealed that no hypothesised cranial module stood out as distinct, as within- and between-module correlations were similar and low, below 0.3 in most cases (see Supporting Information, Table S5). Within-module correlations were considerably lower in the landmark-only dataset compared with the complete shape dataset, whereas between-module correlations were similar across both datasets. Landmark-only analysis therefore suggested the cranium of the Italian fire salamander was only weakly modular, with no cranial regions standing out as highly integrated, distinct modules.

Covariance ratio

Covariance Ratio analysis for the full shape data with the most parametrised model was significant (CR = 0.69, $P = 0.01$) and revealed similar patterns of modularity (Table 3) to those recovered from EMMLi, with CR values closer to 1 for regions related to the

Table 3. Results of the morphological integration of the crania of the fire salamander. The italics diagonal represents the correlation within each cranial region. Above the diagonal, covariance ratio results for the full landmark and semilandmark dataset between the 20 cranial regions. Below the diagonal, EMMLi analysis results for trait correlations (ρ) between the 20 cranial regions (the best supported model) for the full dataset

	PmxD	PmxV	Fr	Par	MaxD	Psph	Sq	Pt	MaxV	Nas	OccD	OC	OccV	OticV	Vom	Qd	Osph	Prf	JJ	OticD
PmxD	*0.46*	0.70	0.62	0.57	0.60	0.57	0.59	0.54	0.54	0.60	0.58	0.55	0.58	0.55	0.61	0.54	0.50	0.53	0.51	0.63
PmxV	0.37	*0.69*	0.66	0.69	0.65	0.61	0.64	0.63	0.68	0.45	0.61	0.60	0.64	0.60	0.67	0.60	0.57	0.51	0.57	0.67
Fr	0.16	0.22	*0.52*	0.88	0.74	0.71	0.78	0.78	0.76	0.65	0.74	0.68	0.74	0.60	0.66	0.78	0.67	0.71	0.74	0.70
Par	0.13	0.22	0.39	*0.57*	0.76	0.76	0.88	0.86	0.76	0.53	0.89	0.77	0.83	0.69	0.67	0.87	0.72	0.57	0.82	0.87
MaxD	0.17	0.26	0.21	0.25	*0.56*	0.79	0.82	0.79	0.89	0.60	0.74	0.67	0.75	0.66	0.74	0.83	0.58	0.65	0.81	0.68
Psph	0.11	0.11	0.13	0.18	0.27	*0.49*	0.80	0.77	0.75	0.62	0.73	0.68	0.78	0.73	0.73	0.81	0.70	0.64	0.78	0.72
Sq	0.14	0.13	0.16	0.22	0.19	0.26	*0.61*	0.87	0.83	0.49	**0.90**	0.80	0.86	0.70	0.71	**0.97**	0.63	0.57	**0.92**	0.88
Pt	0.14	0.12	0.17	0.22	0.24	0.2	0.34	*0.55*	0.76	0.50	0.81	0.72	0.75	0.70	0.68	**0.90**	0.74	0.60	0.83	0.77
MaxV	0.17	0.34	0.3	0.37	0.53	0.26	0.2	0.27	*0.79*	0.50	0.77	0.69	0.77	0.59	0.74	0.84	0.55	0.55	0.79	0.68
Nas	0.14	0.1	0.2	0.15	0.17	0.11	0.1	0.11	0.16	*0.56*	0.47	0.44	0.50	0.50	0.57	0.51	0.48	0.80	0.54	0.46
OccD	0.17	0.16	0.27	0.48	0.34	0.25	0.27	0.3	0.42	0.14	*0.81*	0.89	**0.92**	0.69	0.66	0.89	0.58	0.53	0.85	0.90
OC	0.18	0.14	0.11	0.25	0.3	0.26	0.24	0.23	0.32	0.13	0.64	*0.85*	**0.96**	0.71	0.63	0.77	0.44	0.49	0.74	0.78
OccV	0.18	0.15	0.14	0.26	0.37	0.36	0.26	0.26	0.38	0.13	0.61	0.72	*0.77*	0.77	0.69	0.85	0.52	0.55	0.82	0.82
OticV	0.08	0.1	0.11	0.23	0.24	0.24	0.17	0.14	0.24	0.1	0.36	0.4	0.45	*0.51*	0.66	0.66	0.57	0.57	0.67	0.76
Vom	0.15	0.27	0.15	0.16	0.21	0.19	0.19	0.16	0.27	0.12	0.18	0.14	0.17	0.11	*0.38*	0.70	0.61	0.60	0.65	0.66
Qd	0.15	0.1	0.2	0.21	0.3	0.32	0.57	0.53	0.31	0.11	0.4	0.34	0.42	0.18	0.19	*0.82*	0.66	0.59	**0.97**	0.82
Osph	0.12	0.18	0.25	0.32	0.19	0.26	0.15	0.19	0.23	0.13	0.19	0.08	0.14	0.14	0.15	0.17	*0.61*	0.60	0.57	0.61
Prf	0.13	0.13	0.31	0.17	0.23	0.12	0.1	0.09	0.18	0.28	0.14	0.15	0.16	0.13	0.11	0.09	0.18	*0.64*	0.58	0.52
JJ	0.13	0.09	0.27	0.3	0.33	0.3	0.46	0.48	0.39	0.19	0.5	0.39	0.45	0.18	0.18	0.73	0.25	0.12	*0.89*	0.78
OticD	0.11	0.17	0.2	0.38	0.22	0.15	0.31	0.17	0.28	0.1	0.5	0.35	0.31	0.33	0.17	0.2	0.17	0.12	0.18	*0.55*

Covariance ratio values in bold are greater or equal to 0.9. Abbreviations are as follows: dorsal occipital (OccD), ventral occipital (OccV), occipital condyle (OC), dorsal otic capsule (OticD), ventral otic capsule (OticV), squamosal (Sq), quadrate (Qd), jaw joint (JJ), pterygoid (Pt), parasphenoid (Psph), vomer (Vom), orbitosphenoid (Osph), prefrontal (Prf), ventral maxilla (MaxV), dorsal maxilla (MaxD), dorsal premaxilla (PmxD), ventral premaxilla (PmxV), nasal (Nas), frontal (Fr), parietal (Par).

jaw suspensorium and occipital. Therefore, we find that the regions of the jaw suspensorium (pterygoid, squamosal, quadrate and jaw joint) and the regions of the occipital (dorsal and ventral sides and condyle) are strongly integrated, in concordance with EMMLi analysis, although, unlike EMMLi analysis, the dorsal and ventral sides of the premaxilla are less integrated (CR = 0.7).

Covariance ratio analysis of the landmark-only dataset found significant support for the 15-module model recovered from the landmark-only EMMLi analysis (CR = 0.85, P = 0.01). Covariance ratio values within this model were generally higher than CR values from the full shape dataset, indicating weaker evidence of modularity with the landmark-only dataset. Moreover, many CR values approached or exceeded 1 for several pairs of hypothesised modules, indicating that, despite the significant support for an overall pattern of modularity, CR analysis does not show strong support for most of the hypothesised cranial modules when quantified by landmarks alone (Supporting Information, Table S6).

Morphological disparity

Cranial regions within the jaw suspension module (pterygoid, squamosal, lateral surface of the quadrate and jaw joint regions) exhibited the highest disparity after correcting for landmark number, and the orbitosphenoid exhibited the lowest disparity (Table 4).

For cranial modules, the linear regression of Procrustes variance on integration (within-module correlation) (Fig. 4 and Table 4) was not significant (multiple R^2 = 0.008, adjusted R^2 = -0.081, P = 0.763). Repeating this regression with the original 20 cranial regions revealed a similar, non-significant relationship (multiple R^2 = 0.008, adjusted R^2 = -0.047, P = 0.706) (see Supporting Information, Table S7).

Table 4. Procrustes variances and within-region correlations (ρ) results from EMMLi analysis for the final 13 cranial regions (determined using EMMLi results in Table 3)

Modules	Procrustes variance (x 10^{-7})	Within-region correlations (ρ)
Frontal	12.3	0.52
Maxilla	10.0	0.58
Nasal	6.57	0.56
Occipital	8.59	0.71
Otic, dorsal	9.46	0.55
Otic, ventral	6.70	0.51
Orbitosphenoid	6.07	0.61
Premaxilla	7.22	0.45
Parietal	11.7	0.57
Prefrontal	7.19	0.64
Parasphenoid	6.29	0.49
Suspensorium	14.2	0.52
Vomer	6.44	0.38

DISCUSSION

This study comprehensively sampled the cranial morphology of the Italian fire salamander using a high-dimensional approach, and found a complex pattern of modularity, where the Italian fire salamander cranium comprises 13 modules. This pattern of trait integration was supported from EMMLi analysis with both full data and data subsampled to 10%, as well as with CR analysis. The fire salamander skull therefore comprises multiple, semi-independent regions, with fine-scale, localised variation in functional or developmental influences. The modules we found correspond primarily to individual osteological units, as well as a functional module corresponding to the jaw suspensorium (including the pterygoid, quadrate, jaw joint surface of the quadrate and squamosal regions). The influences of type and timing of ossification do not appear to drive the overall pattern of integration, possibly because the superimposition of multiple sources of covariance can confound each other (Hallgrímsson *et al.*, 2009). However, because genetic, developmental and functional modularity are thought to evolve to match (Wagner & Altenberg, 1996), other developmental or genetic influences than those tested here may act as processes driving the pattern of modularity that we identify. Identifying the pattern of static integration can therefore help identify the drivers of this pattern (i.e. functional or developmental processes) by narrowing down possible factors to those related to the specific patterns observed. The static pattern can also be compared with patterns of integration at the evolutionary and ontogenetic level for determining the factors driving the morphological evolution of salamanders, and for understanding whether our observed pattern of static integration, affected by both developmental and functional pressures, is conserved through evolution.

An absence of distinct developmental modules in the fire salamander cranium is consistent with a previous study of the alpine newt skull (Ivanović & Kalezić, 2010). These results may reflect confounding or overlapping developmental and environmental interactions through ontogeny, or cranial partitioning may have been too simple given the complexity of developmental influences acting on the skull. Ivanović & Kalezić (2010) found no support for any hypothesised modular structure, in contrast to the highly modular pattern that we recover in the fire

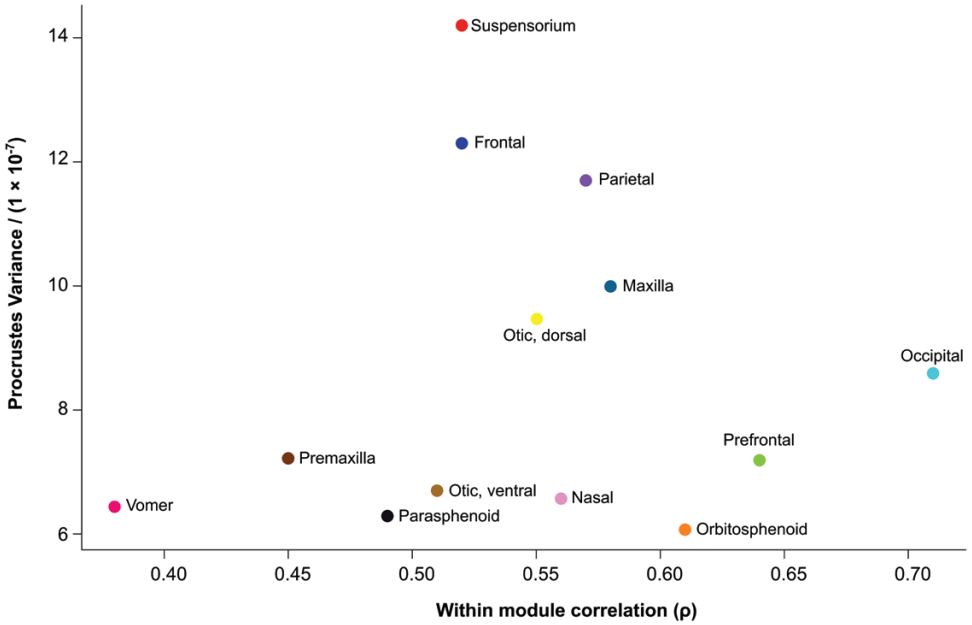

Figure 4. Linear regression of Procrustes variances corrected for landmark number on respective within-module integration. The relationship between the two variables is not significant ($P = 0.76$).

salamander skull. This large discordance may suggest patterns of integration may be highly flexible within different salamander species. Integration can be flexible even within species with different morphs, and can vary through ontogeny (Ivanović *et al.*, 2005), suggesting patterns of integration may be flexible according to life history. However, differences may also be largely attributable to differences in data type and analyses. Ivanović & Kalezić (2010) used two-dimensional landmark data and consequently could not capture shape information for the orbitosphenoid and some bones of the jaw suspension (quadrate and squamosal). In addition, testing hypotheses comprising two to four modules prevented the detection of finer-scale patterns of integration and thus hinders direct comparison between our study and that of Ivanović & Kalezić (2010). Comparison of integration patterns within different subspecies of fire salamander varying in developmental strategy may reveal whether integration patterns are flexible and influenced by developmental strategy.

In contrast, comparing our results to studies implementing a similarly high-dimensional approach reveals instead a surprisingly conserved pattern of integration, particularly within Lissamphibia. The 13-module model we recover in the fire salamander cranium is very similar to the 12- and 13- module models identified intraspecifically within caecilians (Marshall *et al.*, 2019), and to the 10-module model found across the caecilian clade (Bardua *et al.*, 2019b). This similarity is notable given the osteological differences between salamanders and caecilians, which hinders direct comparison. Like Marshall *et al.* (2019), we find that the parasphenoid (analogous to the caecilian ventral os basale) and the vomer form two independent modules, probably due to functional decoupling, the parasphenoid being the floor of the braincase and the vomer being part of the palate (Rose, 2003). Independent palatal and braincase floor regions have also been found across bird and squamate crania (Felice & Goswami, 2018; Watanabe *et al.*, 2019), although across the caecilian clade these regions formed one module (Bardua *et al.*, 2019b). We also find the three regions comprising the occipital bone form one distinct module, despite their functional differences (braincase protection and connection to the vertebral column). A distinct occipital module is also found in caecilian (Bardua *et al.*, 2019b; Marshall *et al.*, 2019), bird (Felice & Goswami, 2018), non-avian dinosaur and crocodylomorph (Felice *et al.*, 2019) crania. The modular structure identified across the fire salamander skull is more strongly concordant with the pattern recovered within caecilians (Bardua *et al.*, 2019b; Marshall *et al.*, 2019) than amniotes, suggesting a possible divergence in modularity patterns between amniotes and amphibians. The similarity of integration patterns between salamanders and caecilians suggests conservation of modularity despite the great diversity of developmental histories and ecologies across these two amphibian clades.

We recover a highly integrated jaw suspensorium module (pterygoid, squamosal, and lateral and jaw joint surfaces of the quadrate) within the fire salamander skull,

likely driven by constraints from feeding mechanics. A highly integrated jaw suspensorium region has also been found across and within caecilians, comprising two strongly correlated modules (quadrate-squamosal and pterygoid) (Bardua *et al.*, 2019b; Marshall *et al.*, 2019). In addition, across birds, the quadrate and pterygoid form a module, although the squamosal belongs to the cranial vault (Felice & Goswami, 2018). This jaw joint region of both caecilians and birds exhibits coordinated movement through kinesis, which may be driving its strong integration (Felice & Goswami, 2018; Bardua *et al.*, 2019b). The highly integrated jaw suspensorium module of the fire salamander may be due to tightly linked, functional constraints in this region related to changing feeding requirements through ontogeny. Fire salamanders experience disparate selective pressures through ontogeny, from larval to adult stages, related to changes in both environment and diet (from water to land), and thus in their feeding mechanism (Shaffer & Lauder, 1988; Wainwright & Reilly, 1994). The highly integrated jaw joint region shared across fire salamanders, caecilians and birds suggests feeding mechanics play a large role in shaping the pattern of integration for these clades.

Data type can have a strong impact on studies of integration. Here, whilst our full landmark and semilandmark dataset recovers a highly modular structure, our landmark-only dataset instead suggests a weakly integrated model, with little to no support for many of the hypothesised cranial modules (despite both methods supporting an overall highly-modular pattern for the cranium). This present study, along with previous comparisons of landmark and semilandmark data to landmark-only data, thus reveals how landmark-only data may exaggerate between-region trait correlations and understate within-region trait correlations (Bardua *et al.*, 2019b; Marshall *et al.*, 2019) resulting in landmark-only datasets recovering weaker support for a modular structure. This is because landmark-only datasets suffer from boundary bias (Goswami *et al.*, 2019) and do not capture shape information along curves and across surfaces, meaning the shape data are not fully representative of a structure. Analyses using semilandmarks may have the opposite effect, due to non-independence of semilandmarks; however, it has been demonstrated in multiple studies that they better capture the morphology of complex structures (Watanabe, 2018; Bardua *et al.*, 2019b; Goswami *et al.*, 2019). Although all methods suffer from biases and artefacts, the improved characterisation of shape achievable with a full landmark and semilandmark dataset likely better reflects the structure of the cranium and the interactions among its regions.

We found no significant relationship between integration and shape variance, and thus no support for the hypothesis that integration facilitates or constrains morphological variance in the fire salamander skull. Our results may thus suggest that integration has limited or variable influence on morphological diversification. Similarly, no significant relationship between integration and variance was recovered intraspecifically within caecilians (Marshall *et al.*, 2019). Similarly, the crania of domestic dogs display a conserved pattern of integration despite a high cranial variance across the entire order (Drake & Klingenberg, 2010). Studies at the macroevolutionary scale have thus far found contrasting patterns, suggesting the relationship between integration and variance is highly flexible across clades, or that the relationship cannot be expressed linearly. Although no significant linear relationship between integration and variance was found across caecilians (Bardua *et al.*, 2019b), high levels of integration are associated with low morphological disparity in the crania of birds and mammals (Goswami *et al.*, 2014; Felice *et al.*, 2018), and conversely, the modular fins of ray-finned fish are highly variable (Larouche *et al.*, 2018). More likely, whether integration promotes or constrains morphological evolution of a module may depend heavily on the alignment of the direction that it facilitates in the morphospace and the direction of selection (Hansen *et al.*, 2011; Goswami *et al.*, 2014; Felice *et al.*, 2018). The heterogeneity of results across studies so far therefore suggests that the relationship between integration and disparity may be complex, with no simple relationship between the two metrics in many, if not most, cases.

With a high-dimensional approach, we analysed the cranial organisation of the Italian fire salamander (*S. salamandra giglioli*). The fire salamander's cranium is highly modular, comprising 13 modules, and this modular organisation is strongly concordant with that recovered in caecilians in terms of both the number and pattern of modules (Bardua *et al.*, 2019b; Marshall *et al.*, 2019). This result suggests a possible conservation of the pattern of integration across lissamphibian crania. We found no support for purely developmental or functional hypotheses of modular organisation, which suggests that the cranial modular pattern in the fire salamander is complex and originates from a mixture of both functional and developmental constraints. Cranial size had little effect on cranial shape in this species, and morphological disparity had no significant relationship with within-module integration, contrary to hypotheses that integration may facilitate or constrain morphological variation. The study of cranial integration of salamanders at the evolutionary level would complement this present study on static integration, providing a more

comprehensive understanding of the intrinsic factors shaping the evolution of the salamander skull.

ACKNOWLEDGEMENTS

We thank Jeffrey W. Streicher at the NHM for giving us access to the collection and helping us with the choice of specimens used in this study. We also thank Vincent Fernandez and Brett Clark for providing training for CT-scanning at the NHM. Finally, we would like to thank three anonymous reviewers for their helpful and insightful comments. This work was funded by the European Research Council (grant STG-2014–637171 to AG). The authors declare no conflicts of interest.

REFERENCES

Ackermann R. 2005. Ontogenetic integration of the hominoid face. *Journal of Human Evolution* **48:** 175–197.

Adams DC. 2016. Evaluating modularity in morphometric data: challenges with the RV coefficient and a new test measure. *Methods in Ecology and Evolution* **7:** 565–572.

Adams DC, **Collyer ML**, **Kaliontzopoulou A. 2019.** *Geomorph: software for geometric morphometric analyses.* R package Version 3.1.0. Available at: https://cran.r-project.org/package=geomorph

Alcobendas M, **Dopazo H**, **Alberch P. 1996.** Geographic variation in allozymes of populations of *Salamandra salamandra* (Amphibia: Urodela) exhibiting distinct reproductive modes. *Journal of Evolutionary Biology* **9:** 83–102.

Bardua C, **Felice RN**, **Watanabe A**, **Fabre A-C**, **Goswami A. 2019a.** A practical guide to sliding and surface semilandmarks in morphometric analyses. *Integrative Organismal Biology* **1:** obz016.

Bardua C, **Wilkinson M**, **Gower DJ**, **Sherratt E**, **Goswami A. 2019b.** Morphological evolution and modularity of the caecilian skull. *BMC Evolutionary Biology* **19:** 30.

Beukema W, **Nicieza AG**, **Lourenço A**, **Velo-Antón G. 2016.** Colour polymorphism in *Salamandra salamandra* (Amphibia: Urodela), revealed by a lack of genetic and environmental differentiation between distinct phenotypes. *Journal of Zoological Systematics and Evolutionary Research* **54:** 127–136.

Bonett RM. 2018. Heterochrony. In: Nuño de la Rosa L, Müller GB, eds. *Evolutionary Developmental Biology*. Cham: Springer, 1–14.

Bonett RM, **Blair AL. 2017.** Evidence for complex life cycle constraints on salamander body form diversification. *Proceedings of the National Academy of Sciences* **114:** 9936–9941.

Bonett RM, **Steffen MA**, **Lambert SM**, **Wiens JJ**, **Chippindale PT. 2013.** Evolution of paedomorphosis in plethodontid salamanders: ecological correlates and re-evolution of metamorphosis. *Evolution* **68:** 466–482.

Botton-Divet L, **Cornette R**, **Fabre A-C**, **Herrel A**, **Houssaye A. 2016.** Morphological analysis of long bones in semi-aquatic mustelids and their terrestrial relatives. *Integrative and Comparative Biology* **56:** 1298–1309.

Brizzi R, **Calloni C. 1992.** Male cloacal region of the spotted salamander, *Salamandra salamandra gigliolii* (Amphibia, Salamandridae). *Bolletino di Zoologia* **59:** 377–385.

Buckley D, **Alcobendas M**, **García-París M**, **Wake MH. 2007.** Heterochrony, cannibalism, and the evolution of viviparity in *Salamandra salamandra*. *Evolution & Development* **9:** 105–115.

Cardini A. 2016. Lost in the other half: Improving accuracy in geometric morphometric analyses of one side of bilaterally symmetric structures. *Systematic Biology* **65:** 1096–1106.

Cheverud JM. 1995. Morphological integration in the saddle-back tamarin cranium. *American Naturalist* **145:** 63–89.

Collar DC, **Schulte JA**, **O'Meara BC**, **Losos JB. 2010.** Habitat use affects morphological diversification in dragon lizards. *Journal of Evolutionary Biology* **23:** 1033–1049.

Da Silva FO, **Fabre A-C**, **Savriama Y**, **Ollonen J**, **Mahlow K**, **Herrel A**, **Müller J**, **Di-Poï N. 2018.** The ecological origins of snakes as revealed by skull evolution. *Nature Communications* **9:** 376.

Dopazo HJ, **Alberch P. 1994.** Preliminary results on optional viviparity and intrauterine siblicide in *Salamandra salamandra* populations from northern Spain. *Mertensiella* **4**:125–138.

Drake AG, **Klingenberg CP. 2010.** Large-scale diversification of skull shape in domestic dogs: disparity and modularity. *The American Naturalist* **175:** 289–301.

Felice RN, **Goswami A. 2018.** Developmental origins of mosaic evolution in the avian cranium. *Proceedings of the National Academy of Sciences* **115:** 555–560.

Felice RN, **Randau M**, **Goswami A. 2018.** A fly in a tube: Macroevolutionary expectations for integrated phenotypes. *Evolution* **72:** 2580–2594.

Felice RN, **Watanabe A**, **Cuff AR**, **Noirault E**, **Pol D**, **Witmer LM**, **Norell MA**, **O'Connor PM**, **Goswami A. 2019.** Evolutionary integration and modularity in the archosaur cranium. *Integrative and Comparative Biology* **59:** 371–382.

Goswami A. 2006. Morphological integration in the carnivoran skull. *Evolution* **60:** 170–180.

Goswami A, **Finarelli JA. 2016.** EMMLi: A maximum likelihood approach to the analysis of modularity. *Evolution* **70:** 1622–1637.

Goswami A, **Lucas T**, **Sivasubramaniam P**, **Finarelli J. 2017.** *EMMLi: A Maximum Likelihood Approach to the Analysis of Modularity*. R package Version 0.0.3. Available at: https://cran.r-project.org/package=EMMLi

Goswami A, **Polly PD. 2010a.** Methods for studying morphological integration and modularity. *The Paleontological Society Papers* **16:** 213–243.

Goswami A, **Polly PD. 2010b.** The influence of modularity on cranial morphological disparity in carnivora and primates (Mammalia) (AW Shingleton, Ed.). *PLoS ONE* **5:** e9517.

Goswami A, **Polly PD**, **Mock OB**, **Sánchez-Villagra MR. 2012.** Shape, variance and integration during craniogenesis: contrasting marsupial and placental mammals. *Journal of Evolutionary Biology* **25:** 862–872.

Goswami A, **Smaers JB**, **Soligo C**, **Polly PD. 2014.** The macroevolutionary consequences of phenotypic integration. *Philosophical Transactions of the Royal Society of London B: Biological Sciences* **369:** 20130254.

Goswami A, **Watanabe A**, **Felice RN**, **Bardua C**, **Fabre A-C**, **Polly PD. 2019.** High-density morphometric analysis of shape and integration: the good, the bad, and the not-really-a-problem. *Integrative and Comparative Biology* 59: 669–683.

Hallgrímsson B, **Jamniczky H**, **Young NM**, **Rolian C**, **Parsons TE**, **Boughner JC**, **Marcucio RS. 2009.** Deciphering the palimpsest: studying the relationship between morphological integration and phenotypic covariation. *Evolutionary Biology* **36:** 355–376.

Hanken J, **Hall BK. 1993.** *The skull. Volume 2 - Patterns of structural and systematic diversity*. Chicago: University of Chicago Press.

Hansen TF, **Pélabon C**, **Houle D. 2011.** Heritability is not evolvability. *Evolutionary Biology* **38:** 258.

Ivanović A, **Kalezić ML. 2010.** Testing the hypothesis of morphological integration on a skull of a vertebrate with a biphasic life cycle: a case study of the alpine newt. *Journal of Experimental Zoology Part B: Molecular and Developmental Evolution* **314B:** 527–538.

Ivanović A, **Kalezić ML**, **Aleksić I. 2005.** Morphological integration of cranium and postcranial skeleton during ontogeny of facultative paedomorphic European newts (*Triturus vulgaris* and *T. alpestris*). *Amphibia-Reptilia* **26:** 485–495.

Klingenberg CP. 2008. Morphological integration and developmental modularity. *Annual Review of Ecology, Evolution, and Systematics* **39:** 115–132.

Klingenberg CP. 2014. Studying morphological integration and modularity at multiple levels: concepts and analysis. *Philosophical Transactions of the Royal Society B: Biological Sciences* **369:** 20130249.

Klingenberg CP. 2016. Size, shape, and form: concepts of allometry in geometric morphometrics. *Development Genes and Evolution* **226:** 113–137.

Klingenberg CP, **Duttke S**, **Whelan S**, **Kim M. 2012.** Developmental plasticity, morphological variation and evolvability: a multilevel analysis of morphometric integration in the shape of compound leaves: morphometric integration in compound leaf shape. *Journal of Evolutionary Biology* **25:** 115–129.

Klingenberg CP, **Marugán-Lobón J. 2013.** Evolutionary covariation in geometric morphometric data: analyzing integration, modularity, and allometry in a phylogenetic context. *Systematic Biology* **62:** 591–610.

Larouche O, **Zelditch ML**, **Cloutier R. 2018.** Modularity promotes morphological divergence in ray-finned fishes. *Scientific Reports* **8:** 7278.

Ledbetter NM, **Bonett RM. 2019.** Terrestriality constrains salamander limb diversification: implications for the evolution of pentadactyly. *Journal of Evolutionary Biology* **32:** 642–652.

Lucas T, **Goswami A. 2017.** *paleomorph: Geometric morphometric tools for paleobiology*. R package Version 0.1.4. Available at: https://cran.r-project.org/package=paleomorph

Marshall AF, **Bardua C**, **Gower DJ**, **Wilkinson M**, **Sherratt E**, **Goswami A. 2019.** High-density three-dimensional morphometric analyses support conserved static (intraspecific) modularity in caecilian (Amphibia: Gymnophiona) crania. *Biological Journal of the Linnean Society* **126:** 721: 742.

Moen DS, **Irschick DJ**, **Wiens JJ. 2013.** Evolutionary conservatism and convergence both lead to striking similarity in ecology, morphology and performance across continents in frogs. *Proceedings of the Royal Society B: Biological Sciences* **280:** 20132156.

Moore WJ. 1981. *The mammalian skull*. Cambridge: Cambridge University Press.

Oslon EC, **Miller RL. 1958.** *Morphological integration*. Chicago: University of Chicago Press.

Porto A, **de Oliveira FB**, **Shirai LT**, **De Conto V**, **Marroig G. 2009.** The evolution of modularity in the mammalian skull I: morphological integration patterns and magnitudes. *Evolutionary Biology* **36:** 118–135.

R Core Development Team. **2019.** *R: A language and environment for statistical computing*. Vienna: R Foundation for Statistical Computing. Available at: https://www.R-project.org/

Randau M, **Goswami A. 2017.** Unravelling intravertebral integration, modularity and disparity in Felidae (Mammalia). *Evolution and Development* **19:** 85–95.

Rohlf FJ, **Slice D. 1990.** Extensions of the procrustes method for the optimal superimposition of landmarks. *Systematic Zoology* **39:** 40–59.

Rose CS. 2003. The Developmental Morphology of Salamander Skulls. In: Heatwole H, Davies M, eds. *Amphibian biology, Vol. 5 Osteology*. Surrey: Beatty & Sons.

Sanger TJ, **Mahler DL**, **Abzhanov A**, **Losos JB. 2012.** Roles for modularity and constraint in the evolution of cranial diversity among *Anolis* lizards. *Evolution* **66:** 1525–1542.

Schlager S. 2017. Morpho and Rvcg – shape analysis in R. In: Zheng G, Li S, Szekely G, eds. *Statistical shape and deformation analysis*. Cambridge: Academic Press. 217–256.

Seidel U, **Gerhardt P. 2016.** *The genus Salamandra: history, biology, systematics, captive breeding. Frankfurt: Edition Chimaira*.

Shaffer HB, **Lauder GV. 1988.** The ontogeny of functional design: metamorphosis of feeding behaviour in the tiger salamander (*Ambystoma tigrinum*). *Journal of Zoology* **216:** 437–454.

Sherratt E. 2011. *Evolution of the caecilian skull*. Manchester: The University of Manchester.

Simon MN, **Marroig G. 2017.** Evolution of a complex phenotype with biphasic ontogeny: Contribution of development versus function and climatic variation to skull modularity in toads. *Ecology and Evolution* **7:** 10752–10769.

Sparreboom M. 2014. *Salamanders of the Old World: the salamanders of Europe, Asia and Northern Africa*. Zeist: KNNV Publishing.

Urošević A, **Ljubisavljević K**, **Jelić D**, **Ivanović A. 2012.** Variation in the cranium shape of wall lizards (*Podarcis* spp.): effects of phylogenetic constraints, allometric constraints and ecology. *Zoology* **115:** 207–216

Urošević A, **Ljubisavljević K**, **Ivanović A. 2019.** Multilevel assessment of the Lacertid lizard cranial modularity. *Journal of Zoological Systematics and Evolutionary Research* **57:** 145–158.

Vidal-García M, **Keogh JS. 2017.** Phylogenetic conservatism in skulls and evolutionary lability in limbs - morphological evolution across an ancient frog radiation is shaped by diet, locomotion and burrowing. *BMC Evolutionary Biology* **17:** 165.

Wagner GP. 1996. Homologues, natural kinds and the evolution of modularity. *American Zoology* **36:** 36–43.

Wagner GP, **Altenberg L. 1996.** Perspective: complex adaptations and the evolution of evolvability. *Evolution* **50:** 967–976.

Wainwright PC, **Reilly SM. 1994.** *Ecological morphology: integrative organismal biology*. Chicago: University of Chicago Press.

Watanabe A. 2018. How many landmarks are enough to characterize shape and size variation? *PloS One* **13:** e0198341.

Watanabe A, **Fabre A-C**, **Felice RN**, **Maisano JA**, **Müller J**, **Herrel A**, **Goswami A. 2019.** Ecomorphological diversification in squamates from conserved pattern of cranial integration. *Proceedings of the National Academy of Sciences* **116:** 14688–14697.

Willmore KE, **Leamy L**, **Hallgrimsson B. 2006.** Effects of developmental and functional interactions on mouse cranial variability through late ontogeny. *Evolution & Development* **8**:550–567.

Zelditch ML. 1988. Ontogenetic variation in patterns of phenotypic integration in the laboratory rat. *Evolution* **42**:28–41.

Zelditch ML, **Carmichael AC. 1989a.** Growth and intensity of integration through postnatal growth in the skull of *Sigmodon fulviventer*. *Journal of Mammalogy* **70:** 477–484.

Zelditch ML, **Carmichael AC. 1989b.** Ontogenetic variation in patterns of developmental and functional integration in skulls of *Sigmodon fuliviventer*. *Evolution* **43**:814–24.

SUPPORTING INFORMATION

Additional Supporting Information may be found in the online version of this article at the publisher's website:

Table S1. List of the specimens used in this study.
Table S2. Landmark and curve definitions.
Table S3. Centroid sizes of the specimens.
Table S4. EMMLi analysis results on average random 10% subsampling.
Table S5. EMMLi analysis results on landmark only dataset.
Table S6. Covariance Ratio results on landmark only dataset.
Table S7. Procrustes variances and within-region correlations for the 20 cranial regions.

SHARED DATA

All the reconstructed meshes of the salamanders used in this study are available on https://phenome10k.org/scans/?q=Salamandra+salamandra+gigliolii. Landmark data are available on https://www.goswamilab.com/software.